DOI 10.59887/2073-6673.2025.18(2)-2

EDN EEVAUM

УДК 551.465

© *V. V. Ivanov*[1,2]*, *A. V. Danshina*[2], *A. V. Smirnov*[2], 2025
© Translated from Russian: *E.S. Kochetkova*, 2025
[1]Lomonosov Moscow State University, 1 Leninskie Gory, Moscow, 119991, Russia
[2]Arctic and Antarctic Research Institute, 38 Bering Str., St. Petersburg, 199397, Russia
*vladimir.ivanov@aari.ru

Spatiotemporal Structure and Variability of Thermohaline Parameters in the Intermediate Water Layer North of the Severnaya Zemlya Archipelago

Received 26.10.2024, Revised 22.04.2025, Accepted 12.05.2025

Abstract

Time series of water temperature and conductivity obtained over three years of continuous measurements at seven autonomous moored stations north of the Severnaya Zemlya archipelago located in the Arctic Basin of the Arctic Ocean were analyzed in combination with numerical modeling to investigate the spatiotemporal variability of temperature and salinity in the intermediate layer of Atlantic-origin waters. These waters propagate along the Eurasian continental slope within the Arctic Boundary Current (ABC). Within 85 km of the shelf edge, three distinct branches of Atlantic Water (AW) transport were identified, each characterized by a unique origin history of origin that shapes the variability of its thermohaline properties. The most energetic mode of temporal variability at all stations is associated with oscillations with a period of approximately 12 months. The amplitude of these oscillations decreases with increasing distance from the shelf edge, while their phase differs among the AW branches. Numerical modeling indicates that, in the study region, the typical phase–distance relationship observed in the western Nansen Basin is disrupted by the large-scale input of cold, freshened water through the St. Anna Trough.

Keywords: Arctic Ocean, water masses, sea currents, thermohaline parameters, seasonal variability, numerical models

© *В. В. Иванов*[1,2]*, *А. В. Даньшина*[2], *А. В. Смирнов*[2], 2025
[1]Московский государственный университет им. М.В. Ломоносова, 119991, г. Москва, Ленинские горы, д. 1
[2]Арктический и антарктический научно-исследовательский институт, 199397, г. Санкт-Петербург, ул. Беринга, д. 38
*vladimir.ivanov@aari.ru

Пространственно-временная структура и изменчивость термохалинных параметров в промежуточном слое вод к северу от архипелага Северная Земля

Статья поступила в редакцию 26.10.2024, после доработки 22.04.2025, принята в печать 12.05.2025

Аннотация

Временные серии температуры и электропроводности воды, полученные за три года непрерывных измерений на семи автономных буйковых станциях к северу от архипелага Северная Земля в Арктическом бассейне Северного Ледовитого океана, проанализированы совместно с данными численного моделирования с целью

Ссылка для цитирования: *Иванов В.В.*, *Даньшина А.В.*, *Смирнов А.В.* Пространственно-временная структура и изменчивость термохалинных параметров в промежуточном слое вод к северу от архипелага Северная Земля // Фундаментальная и прикладная гидрофизика. 2025. Т. 18, № 2. С. 19–40. https://doi.org/10.59887/2073–6673.2025.18(2)-2 EDN EEVAUM
For citation: *Ivanov V.V.*, *Danshina A.V.*, *Smirnov A.V.* Spatiotemporal Structure and Variability of Thermohaline Parameters in the Intermediate Water Layer North of the Severnaya Zemlya Archipelago. *Fundamental and Applied Hydrophysics*. 2025;18(2):19–40. https://doi.org/10.59887/2073–6673.2025.18(2)-2

изучения пространственно-временной изменчивости температуры и солености в промежуточном слое вод атлантического происхождения, распространяющихся вдоль континентального склона Евразии в потоке Арктического пограничного течения. В пределах 85-ти км от бровки шельфа выделено три ветви переноса атлантической воды, каждая из которых характеризуется своей предысторией, определяющей изменчивость их термохалинных параметров. Наиболее энергоемкая мода временной изменчивости на всех автономных буйковых станциях определяется колебаниями с периодом около 12 мес., амплитуда которых уменьшается по мере удаления от бровки шельфа, а фаза различна в разных ветвях атлантической воды. Данные численного моделирования показали, что в районе постановки автономных буйковых станций зависимость фазы колебаний от расстояния до пролива Фрама, характерная для западной части бассейна Нансена, нарушается массированным поступлением охлажденной/распресненной воды через желоб Св. Анны.

Ключевые слова: Северный Ледовитый океан, водные массы, морские течения, термохалинные параметры, сезонная изменчивость, численные модели

1. Introduction

In September 2018, during the international expedition “Arctic-2018” aboard the R/V Akademik Tryoshnikov, seven autonomous moored stations (AMS) were successfully recovered. These stations had been deployed in September 2015 along the continental slope and adjacent deep-water region of the Arctic Basin (AB) of the Arctic Ocean, north of the Severnaya Zemlya archipelago. The deployment was part of a study aimed at investigating the spatiotemporal variability of the intermediate layer occupied by Atlantic-origin water commonly referred to as Atlantic Water in the Arctic Ocean [1] as it flows along the Eurasian continental slope (Fig. 1).

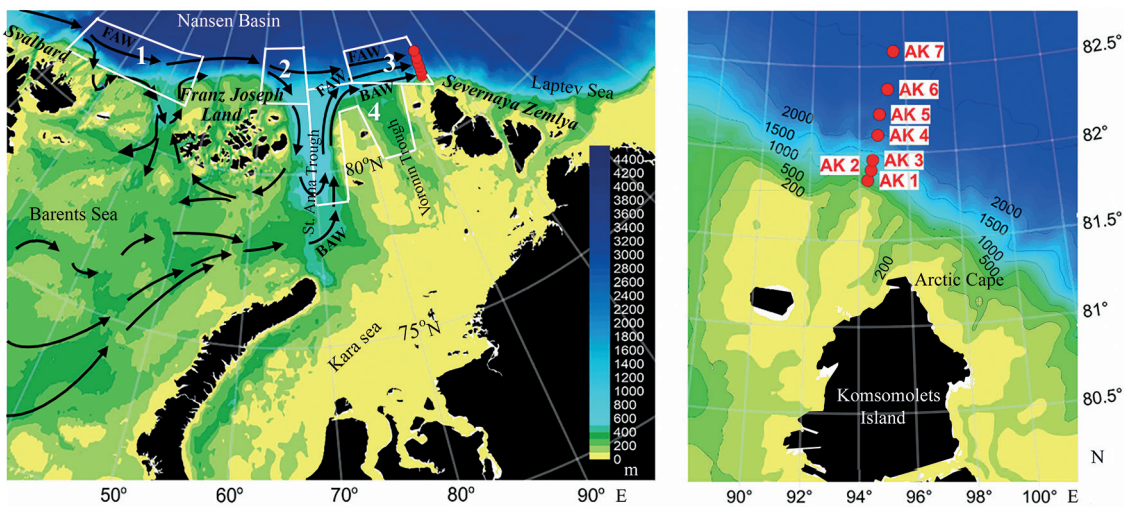

Fig. 1. Bottom topography of the eastern Atlantic sector of the Arctic Ocean (left) [2]. Locations of the AMS (right). Numbers (1–4) indicate regions referenced in the analysis in Section 5. Main pathways of AW transport are shown by black arrows

Warm and saline waters from the Atlantic Ocean enter the Arctic Ocean (AO) via the Norwegian Current, which is a continuation of the North Atlantic Current (NAC). In the North European Basin of the AO, the Norwegian Current splits into the West Spitsbergen Current (WSC) and the Nordkapp Current (NCaC). The WSC enters the Arctic Basin (AB) through Fram Strait, while the NCaC flows through the Barents Sea and the St. Anna Trough in the northern Kara Sea [3, 4]. After passing through Fram Strait, Atlantic Water (AW) carried by the WSC rapidly cools and freshens in its upper layer due to atmospheric heat loss and vertical mixing with less dense Arctic surface waters and meltwater from sea ice [5]. The lower portion of the AW, which escapes vertical mixing, forms what is commonly referred to as Fram Atlantic Water (FAW). In the western Nansen Basin, FAW retains thermohaline properties close to those observed in the year-round ice-free northeastern Fram Strait [6]. This water mass subsequently spreads as an intermediate layer (150–900 m) with positive temperature along the continental slope of Eurasia and North America within the Arctic Boundary Current (ABC),

forming large-scale cyclonic gyres over the deep basins of the AB [6]. In contrast, AW entering the Barents Sea via the NCaC spreads northeastward throughout the entire water column [7]. In winter, thermohaline convection cools and freshens the upper 100–150 m of the AW, while its bottom layer is modified by isopycnal mixing with cold, dense waters formed over the shallow northwestern shelf of the Novaya Zemlya archipelago [8]. As a result, a modified water mass with lower temperature and salinity compared to the original AW commonly referred to as Barents Sea Atlantic Water (BAW) reaches the northeastern Barents Sea [6, 7]. BAW enters the AB through the St. Anna Trough as a density-driven flow, where it converges with Fram Atlantic Water. However, full mixing of these two AW-derived water masses does not occur in the contact zone due to their significant density contrast. Most of the BAW underflows the FAW, and a narrow frontal zone forms between the shelf and the continental slope. This frontal zone is a site of intense turbulent exchange of heat and salt [9, 10] (Fig. 2).

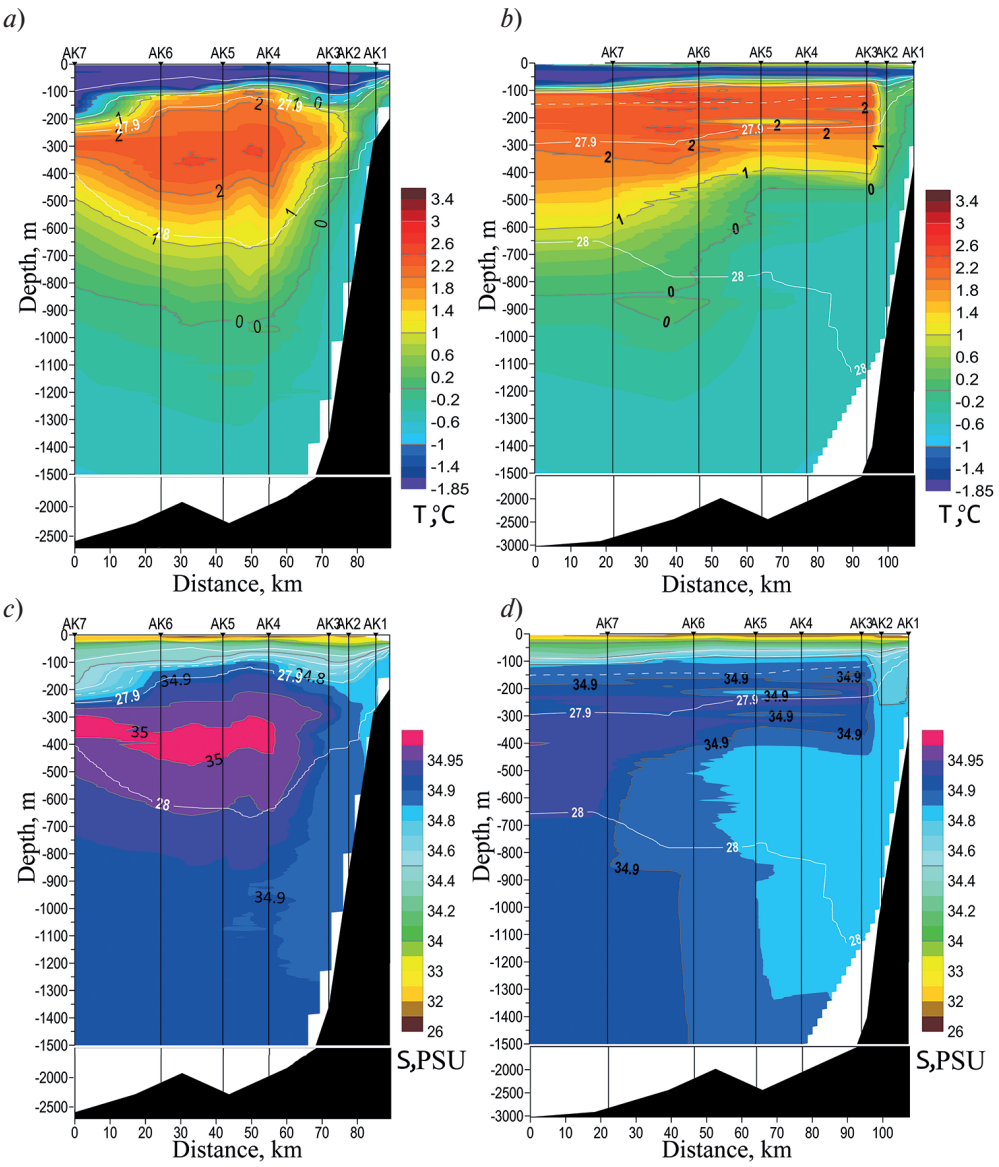

Fig. 2. Vertical distribution of potential temperature (°C; *a*, *b*) and salinity (PSU – Practical Salinitu units; *c*, *d*) in the 0–1500 m layer along the transect crossing the AMS array in September 2015 and 2018, respectively (based on data from R/V Akademik Tryoshnikov cruises). Anomalies of potential density (deviations from 1000 kg/m³) are shown as white contours. Locations of the AMS along the transect are indicated on the top axis

Interest in AW in the AO has increased markedly since the early 1990s, following a sustained rise in the temperature of FAW [11–13]. This interest was further fueled by the development of long-term observation technologies, particularly AMS deployable beneath drifting ice [14]. The use of AMS played a key role in confirming the hypothesis [5] that explains the submergence of FAW east of Fram Strait by vertical mixing, which cools and freshens its upper layer [15, 16]. Long-term measurements of thermohaline properties at AMS deployed along the continental slope have also made it possible to trace the propagation of thermohaline anomalies carried into the AO by the North Atlantic Current (NAC) [13, 17–19], and to identify intra-annual (seasonal) temperature oscillations with a period of approximately 12 months and amplitudes reaching up to 2 °C along the path of the Arctic Boundary Current (ABC) from Fram Strait to the southern extensions of the Lomonosov Ridge [15, 20–26]. The prevailing hypothesis attributes the seasonal temperature variability in FAW to its generation in the ice-free Fram Strait due to seasonal changes in air–sea heat exchange, followed by downstream advection along the ABC [15, 27]. Additional mechanisms proposed to explain the spatiotemporal variability of FAW thermohaline properties include wind-driven upwelling [25], isopycnal mixing with dense shelf waters [28], displacement of the frontal zone between FAW and Barents Sea Atlantic Water, and ocean sea level fluctuations [24]. In contrast, available data on the temporal variability of thermohaline properties in BAW remain sparse and contradictory, owing to limited wintertime observations in the northeastern Barents Sea and the St. Anna Trough. According to year-long AMS measurements conducted in the northeastern Barents Sea during 1990–1991, seasonal temperature variability in BAW was found to be small, approximately 0.2 °C [7].

In contrast, year-long AMS observations in the St. Anna Trough during 2009–2010 revealed seasonal temperature variations in the BAW core exceeding 1 °C [29]. Multiscale temperature variability in BAW was also identified from AMS records in the AB [26, 29, 30]. With the exception of [26], this variability was attributed to changing formation conditions of BAW associated with variations in sea-ice cover in the northeastern Barents Sea, and was not linked to seasonal cycles. Hereafter, the abbreviation AW is used when it is necessary to distinguish Atlantic-origin water from other water masses in the AB. When referring to the individual branches of AW with distinct transformation histories, the abbreviations FAW and BAW are used.

Study [26] analyzed the structure and variability of the ABC in the confluence zone of FAW and BAW based on instrumentally measured temperature and current data interpolated onto a regular spatial grid from AMS records. The present paper offers results from an alternative methodological approach based on statistical analysis of the original time series of thermohaline properties. Structural inferences about the ABC from [26] are used as a reference for interpreting the patterns identified here. Section 2 describes the data sources, including three years of in situ temperature and conductivity measurements from seven long-term AMS deployments, hydrographic transects intersecting the AMS locations (see Figs. 1 and 2), and numerical simulations using the NEMO model (Nucleus for European Modelling of the Ocean) [31]. Sections 3 and 4 present the analysis of temperature and salinity time series derived from observations and modeling, with statistical estimates of their spatiotemporal variability. Section 5 places the results from the localized region north of the Severnaya Zemlya Archipelago into the broader context of AW transport and transformation across the eastern Atlantic sector of the AO, based on the modeling data. The main findings are summarized in the final section.

2. Materials and Methods

The challenge of extracting physically meaningful insights from in situ observational data for the purpose of objectively describing the structure and variability of hydrographic fields in the ocean stems from the spatial fragmentation of observations and their restriction to fixed time intervals. In contrast, numerical modeling and ocean reanalysis products enable reconstruction of a spatially continuous picture of hydrographic field structure and variability, with spatial resolution defined by the model grid and temporal coverage matching the integration period. However, numerical simulations and reanalysis data cannot yet fully replace in situ observations due to limitations in model resolution and the use of simplified parameterizations for subgrid-scale processes. Consequently, combining the strengths of different observational and modeling approaches offers the most robust strategy for documenting the spatiotemporal variability of ocean hydrographic structure.

2.1. In situ observational data

Autonomous moored stations (AMS) are a well-established observational platform that enables long-term monitoring of key marine environmental parameters. In ice-free regions of the global ocean, AMS permanently deployed at fixed locations have been widely used since the latter half of the 20th century. In the AO, widespread use of AMS began in the 2000s, facilitated by technological advances that made it possible to deploy them in a subsurface configuration, with the upper buoy positioned 50–100 m below the sea ice, as well as to locate and recover the systems under continuous ice cover. All AMS recovered from the study region shared a common design: the primary buoy was placed at a depth of 40–60 m and supported the entire sensor array. Instruments were mounted along the mooring line and included, depending on the station, MicroCAT SBE37 [32] CTDs for point measurements of temperature, conductivity, and pressure, and acoustic Doppler current profilers (ADCPs) for measuring current speed and direction throughout the water column. Auxiliary components essential for deployment and recovery such as acoustic transponders, release mechanisms, and a concrete anchor ensured stable positioning of the AMS at the intended site. The main dataset used in this study consisted of 15-minute records of temperature and conductivity (converted to PSU) from the MicroCAT SBE37 [32], with accuracies of 0.002 °C and 0.03 mS/cm, respectively. Additional information was obtained from CTD profiles measured during deployment and recovery using a SeaBird SBE19plus probe, with measurement accuracies of 0.005 °C and 0.05 mS/cm, respectively.

The time series of measurements recorded at the AMS and uploaded to the database were subjected to additional processing. Some of the salinity records contained segments with evident outliers (≥1 PSU) that could not be corrected through physical interpretation. If such outliers occurred at the beginning or end of a record, those segments were removed and the truncated record was retained for further analysis. Records with outliers distributed throughout the time series were excluded from subsequent use. The raw data were checked for possible outliers defined as values exceeding twice the standard deviation from a 1-month moving average after which suspect data points were replaced by linearly interpolated values. The total proportion of corrected values reached approximately 7 % in salinity and less than 4 % in temperature records. Daily averaging was then applied. To minimize the effects of instrument depth shifts, measurements taken at depths exceeding 40 m from the instrument's shallowest depth were replaced with linearly interpolated values. The resulting temperature and salinity time series, with a daily temporal resolution, were used in the subsequent analysis.

Unfortunately, a significant portion of salinity records that passed the above formal screening procedure showed substantial discrepancies up to 0.15 PSU when compared with CTD profiles collected during AMS deployment and recovery. If such salinity time series also exhibited weak correlation with the corresponding temperature series and/or showed implausible trends resembling sensor conductivity drift, they were deemed unreliable and excluded from analysis.

2.2. NEMO model

The NEMO v3.6 model [33] is based on the full set of equations for incompressible fluid motion, incorporating the traditional hydrostatic and Boussinesq approximations. The model supports multiple coordinate systems spherical, Cartesian, and curvilinear. This flexibility allows NEMO to be implemented in both global and regional configurations, including domains with curvilinear grids, thereby enabling adequate resolution of surface and bottom boundary layers. The model also allows coupling with global atmospheric circulation models for external forcing, and includes modules for simulating sea ice dynamics and biogeochemical transformations. For the present study, a configuration of NEMO adapted to pan-Arctic conditions was used, incorporating the LIM3 sea ice model [34]. Vertical diffusion and viscosity were parameterized using the Generic Length Scale (GLS) turbulence closure scheme [33]. Horizontal mixing was implemented using a Laplacian operator for tracers and a biharmonic operator for momentum, with Smagorinsky-type parameterization [33]. To specify boundary conditions at the two open boundaries of both the oceanic and sea ice components, as well

as at the ocean–atmosphere interface, reanalysis products were used: the global ocean reanalysis GLOBAL_MULTIYEAR_PHY_001_030 [35] and the atmospheric reanalysis ERA5 [36]. Tidal forcing at the open boundaries was prescribed using data derived from simulations with the inverse tidal model TPXO7.2 [37]. Initial temperature and salinity fields in the model domain were based on climatological data from the World Ocean Atlas 2018 (WOA18) [38], which were interpolated onto the nodes of the model's orthogonal curvilinear grid with a horizontal resolution of 4–8 km. Bathymetry at the grid nodes was obtained from the GEBCO global depth database [2].

2.3. Wavelet analysis

To quantitatively assess the cyclic variability in the observed and modelled time series of temperature and salinity, wavelet transform analysis was applied. Compared to conventional harmonic analysis, wavelet transform offers a key advantage in its ability to detect local cycles whose parameters vary over time a common feature in hydrographic time series. The wavelet transform decomposes the original signal into a set of basis functions, each of which is localized in both frequency (or temporal scale) and time, thereby enabling time-resolved spectral analysis. In this study, a Morlet wavelet was used to analyze the temporal variability of thermohaline characteristics at the AMS. The Morlet wavelet consists of a plane wave modulated by a Gaussian envelope and was applied with a dimensionless central frequency of 6 [39].

3. Vertical water structure

Vertical profiles of temperature, salinity, and potential density anomaly during the deployment (September 2015) and recovery (September 2018) of the AMS are shown in Fig. 2. These profiles indicate that the vertical structure of the water column in the study area remains relatively stable on an interannual timescale. Characteristic hydrographic zones typical of the region [3] are clearly distinguishable in both temperature and salinity. The surface layer (0–20 m) is occupied by warmed (T = –0.2 to 0.2 °C) and freshened (S = 31–33 PSU) waters, resulting from seasonal radiative heating and sea ice melt. Beneath this lies the cold halocline layer [5], extending to depths of 80–100 m, where salinity increases by several units while temperature remains nearly constant and close to the freezing point. Below the halocline is the intermediate layer occupied by FAW, with its upper boundary marked by a pronounced thermocline across which temperature increases by several degrees.

As noted above, FAW is conventionally identified by its positive temperature [1]. Accordingly, in the study area, its upper and lower boundaries at AK4–AK7 are located at depths of 80–100 m and 800–900 m, respectively. The core of the FAW, centered at 200–300 m, is characterized by temperatures of 2.2–2.4 °C and salinities of 34.9–35.0 PSU. At AK1 and AK2, BAW occupies the entire water column beneath the cold halocline, with temperatures ranging from –0.5 to +0.5 °C and salinities of 34.86–34.88 PSU. At AK4–AK6, BAW is found between the FAW and the deeper water mass, which is characterized by negative temperatures and salinities of 34.90–34.91 PSU. In the vicinity of AK3, a sharp frontal zone separates FAW and BAW. In 2018, between AK2 and AK3, a distinct frontal interface was observed in the 100–400 m depth range, with horizontal gradients of $\Delta T = 0.34$ °C/km and $\Delta S = 0.03$ PSU/km.

Despite the overall similarity in the vertical water structure between 2015 and 2018, some notable differences are evident. The surface layer in September 2018 was significantly warmer than in September 2015. In 2018, temperatures in the surface layer were above 0 °C throughout the entire section, whereas in 2015 the surface layer was predominantly below 0 °C, with values close to the freezing point along most of the transect. This contrast is likely due to the earlier northward retreat of the ice edge in summer 2018 compared to summer 2015 [40], which resulted in more intense radiative heating. The cold halocline layer in September 2015 was, on average, twice as thick as in 2018, with its lower boundary in the deep basin extending below 100 m. In 2015, the layer occupied by FAW was spatially confined to the area between AK3 and AK5, whereas in 2018 it extended from AK3 to the deep end of the section. The maximum temperature in the FAW core in 2018 (~2.5 °C) was slightly higher than in 2015 (~2.3 °C), while its salinity was markedly lower: 34.94 PSU compared to 35.02 PSU

in 2015. The area occupied by BAW in 2018 was considerably larger than in 2015, and its salinity (34.83–34.85) was lower than in 2015 as well. The described features of the vertical water structure during the deployment and recovery of the AMS were taken into account in subsequent analyses to assess the reliability of the data obtained from the AMS (see Section 2.1).

4. Spatiotemporal variability of thermohaline properties in the AW layer

To quantitatively describe the spatiotemporal variability of thermohaline parameters in the intermediate layer of Atlantic-origin water, a comparative analysis of temperature and salinity time series was conducted in both horizontal and vertical dimensions. The results are presented in the following two subsections. Figure 3 shows the mean profiles of temperature and salinity at all AMS locations, constructed using data from depth levels that successfully passed the preliminary quality control (see Section 2.1).

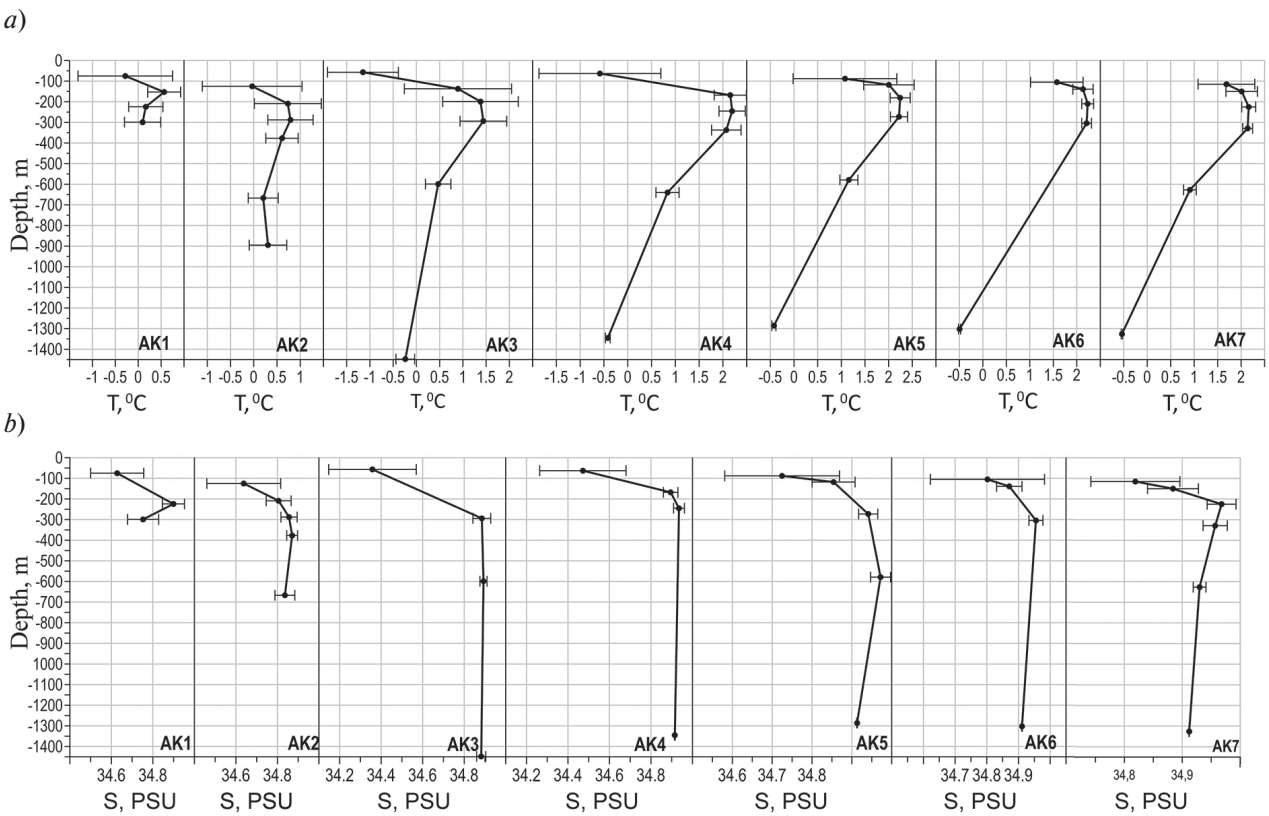

Fig. 3. Mean vertical profiles of temperature (°C; *a*) and salinity (PSU; *b*), averaged over the records at the AMS. Horizontal lines indicate standard deviation (SD)

As shown in the figure, the strongest temporal variability is observed in the upper layers, at depths shallower than 200 m, with the amplitude of variability decreasing toward the deep basin. Considering that the temperature maximum across all AMS (except AK1) is generally located near the 300 m horizon (Fig. 3), time series from levels close to 300 m were selected for the analysis of temporal variability at the different AMS sites.

4.1. Temporal variability of thermohaline parameters at the temperature maximum level across different AMS

Time series of temperature and salinity at the level of maximum water temperature (see Figs. 2 and 3) from all AMS sites are presented in Fig. 4. At AK2–AK5, a pronounced annual cycle is evident in both temperature

and salinity records from 2015 to 2017, with synchronized extrema: minima in April–June and maxima in November–December. In 2018, this pattern is disrupted: a maximum is observed in May instead of the expected minimum. This anomaly is likely associated with the passage of a temperature/salinity disturbance not linked to the annual cycle. This is evident from the fact that, similar to the previous two years, a seasonal decline in temperature and salinity is observed at the beginning of 2018; however, this trend is interrupted at the end of March by a sharp increase in both parameters, culminating in a maximum in April–May. The duration of these thermohaline extremes is asymmetrical relative to the mean. Both temperature and salinity minima are more distinct and short-lived, lasting from one month (AK2, AK5) to two and a half months (AK3, AK4). In contrast, maxima are smoother and more prolonged: the period during which temperature and salinity remain near their peak values ranges from three months (AK5) to eleven months (AK3). Overall, at AK2–AK5, the annual cycle is characterized by alternating intervals of gradual increase/decrease and rapid drop/rise in thermohaline parameters.

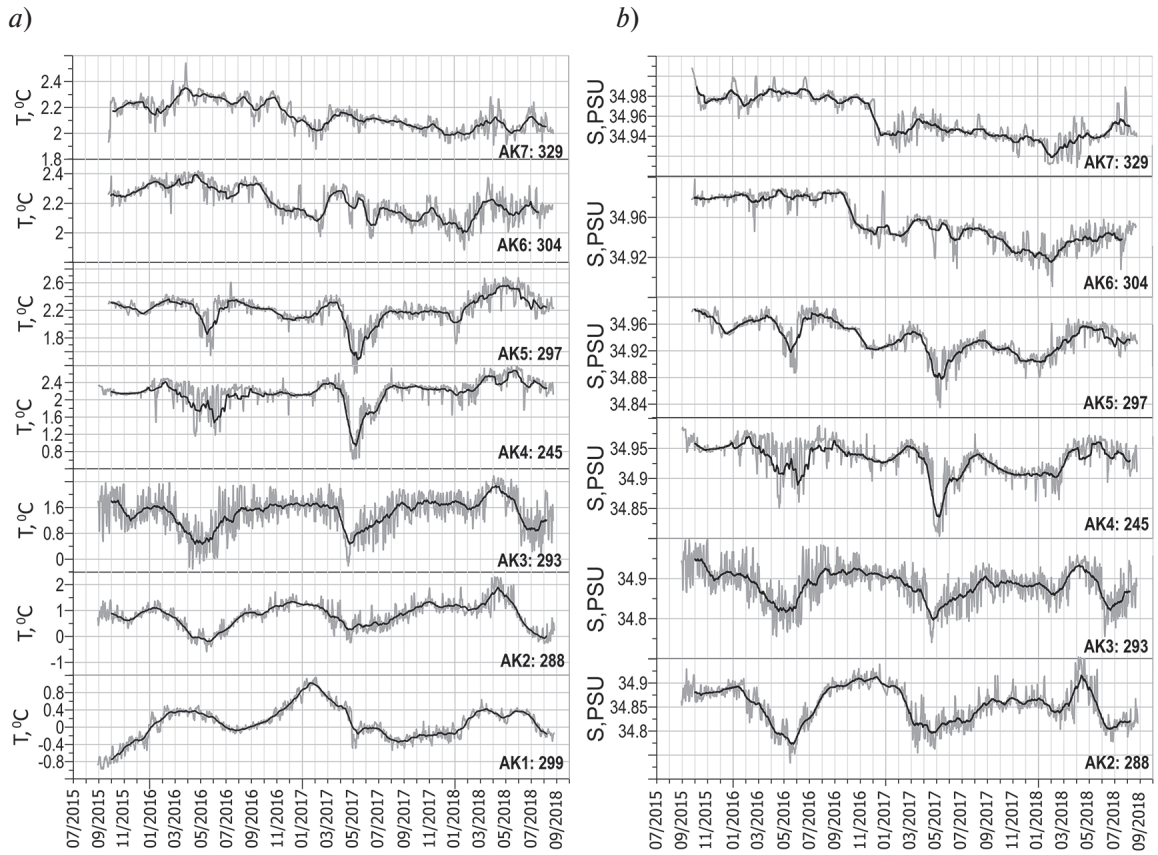

Fig. 4. Time series of temperature (*a*) and salinity (*b*) in the AW layer (mooring IDs and measurement depths are indicated in the figure). Bold lines show a 1-month moving average. *Note*: the salinity time series at 299 m was discarded (see subsection 2.1 for details)

At the deep-water AMS AK6 and AK7, annual variability in temperature and salinity is also evident, though much less pronounced than at AK2–AK5. Moreover, the phase of the annual cycle is nearly opposite: minima occur in November–December, and maxima in April–May. Another key distinction in the AK6 and AK7 records, relative to those from shallower AMS, is the presence of a clear negative trend in both temperature and salinity. A sharp salinity drop (by 0.04 PSU), less pronounced in temperature, is observed at AK6 and AK7 between October and December 2016. A somewhat smaller but still noticeable salinity decrease occurred over the same period at AK5 and AK4. In spring and summer 2018, AK6 and AK7 also show an increase in temperature

and salinity, similar to that observed at AK2–AK5 and previously attributed to a thermohaline anomaly. However, at the two deep-water AMS, this increase also aligns with the phase of the annual cycle and may therefore not be linked to the anomaly detected at AK2–AK5.

The temperature record at the shallowest AMS, AK1, also exhibits a clear annual cycle, but with a phase shift relative to all other AMS: the maximum occurs in February–March, and the minimum in August–September. Unlike the records from other AMS, the durations of the temperature extrema at AK1 are comparable. During the first half of the record (up to early 2017), a pronounced positive trend is observed, which reverses after the temperature peak in February 2017. Since the instruments at all measured levels on AK1 recorded parameters characteristic of BAW (see Figs. 2 and 3), it is unsurprising that the patterns of temporal variability in thermohaline parameters at this AMS differ from those at AK4–AK7, where instruments deployed near 300 m were likely located within FAW. Referring to Fig. 2, it can be seen that on neighboring AMS AK2 and AK3, the deep instruments (667 and 599 m) were positioned in BAW from the outset of the measurements, while by the time of AMS recovery, deep instruments on AK4 (640 m) and AK5 (579 m) were also found within BAW. Potential links among these records are examined in the following subsection.

To quantitatively assess the degree of spatial coherence in the temperature and salinity time series, cross-correlation coefficients were calculated for both daily values and time series smoothed with a moving monthly mean. The results are presented in Table 1. The significance level for all correlation coefficients (1 — p value) exceeds 0.99.

Table 1

Cross-correlation coefficients for temperature series (above the diagonal) and salinity series (below the diagonal)

AMS	AK1–299 m	AK2–288 m	AK3–293 m	AK4–245 m	AK5–297 m	AK6–304 m	AK7–329 m
AK1	1	0.11/0.16	–0.02/–0.02	0.08/0.06	0.11/0.08	0.00/0.00	–0.02/0.01
AK2	–	1	**0.65/0.91**	0.35/**0.53**	0.22/0.34	–0.33/–0.38	–0.37/–0.47
AK3	–	**0.62/0.89**	1	0.39/**0.68**	0.25/**0.50**	–0.25/–0.35	–0.29/–0.47
AK4	–	0.28/0.46	0.34/**0.63**	1	**0.62/0.82**	–0.07/–0.19	–0.21/–0.41
AK5	–	0.20/0.26	0.27/0.48	**0.65/0.78**	1	0.11/0.14	0.01/–0.03
AK6	–	0.03/–0.01	0.07/0.12	0.41/0.41	**0.60/0.71**	1	**0.67/0.84**
AK7	–	0.02//0.02	0.07/0.12	0.34/0.36	**0.54/0.66**	**0.82/0.93**	1

Note: "X/Y" indicates the correlation coefficient values for the daily and smoothed time series, respectively.

High positive correlations in both temperature and salinity time series are observed among AK2–AK5. For time series smoothed with a monthly moving average, the correlation coefficients mostly exceed 0.5, indicating strong coherence in the low-frequency range. A similarly strong positive correlation between temperature and salinity is found at the deepest AMS–AK6 and AK7. In contrast, correlations between AK2–AK4 and AK6–AK7 are negative and relatively high in absolute value (–0.3 to –0.4). A somewhat unexpected result is the near absence of correlation between temperature series at AK5 and AK6–AK7, despite strong correlations in the corresponding salinity series (above 0.5). This discrepancy can be attributed to pronounced negative trends in the salinity series at these three stations. After removing the linear trend, the correlation between daily salinity series at AK5 and AK6 drops to 0.41, and to 0.33 between AK5 and AK7. Correlations between temperature variability at AK1 and the rest of the AMS are close to zero, indicating a near-complete decoupling between the processes governing temperature variability in the BAW and those in the FAW core in the deep basin.

Based on the analysis presented in this section, it can be assumed that within 85 km northward from the shelf break off the Severnaya Zemlya Archipelago, three distinct branches of AW are present, each is characterized by its own variability patterns. Directly at the shelf break (AK1), BAW is observed, flowing into the Nansen Basin

from the Kara Sea along the eastern slope of the St. Anna Trough [29]. Farther offshore (AK2–AK5), the water mass consists of FAW that has recirculated within the St. Anna Trough [9]. In the deep part of the section (AK6–AK7), FAW is present that has not entered the St. Anna Trough and therefore has traveled a shorter distance along the continental slope. As a result, this branch retains higher mean temperature and salinity (see Fig. 4). AMS AK2 and AK5 are likely situated near the boundaries between different AW branches, and are therefore influenced by waters of varying origin and history. As previously noted, all AMS show well-pronounced intra-annual oscillations with varying phase and amplitude. A more detailed discussion of the cyclicity in temperature and salinity records is presented in Section 4.3, where the observational data from AMS are compared with model results

4.2. Temporal variability of thermohaline properties in the AW layer: vertical structure

Time series of temperature and salinity in FAW that presumably recirculated within the St. Anna Trough (AK2) and in the outer branch of FAW (AK7), which was not affected by shelf processes, are shown in Fig. 5 and 6.

At AK2, the previously identified intra-annual cycle is evident at all depths. On the three upper levels (125, 209, and 288 m), the phase of the cycle is nearly identical for both temperature and salinity: maximum values are reached in November and persist until February, followed by a decline to minimum values in May–June. At 353 m, which lies below the FAW core, temperature extremes occur 1–2 months later, whereas the salinity phase remains consistent with that of the overlying layers. In the lower part of the Atlantic layer (667 m), temperature maxima and minima are shifted further in time toward March–April and July–August, respectively. In spring 2018, all levels recorded a synchronous increase in both temperature and salinity, disrupting the regular annual cycle a signal that was also observed in the Atlantic layer at other AMS. This event was likely caused by the passage of a positive thermohaline anomaly that originated upstream in the Nordic Seas or the Atlantic Ocean, a phenomenon documented in previous years [13, 18].

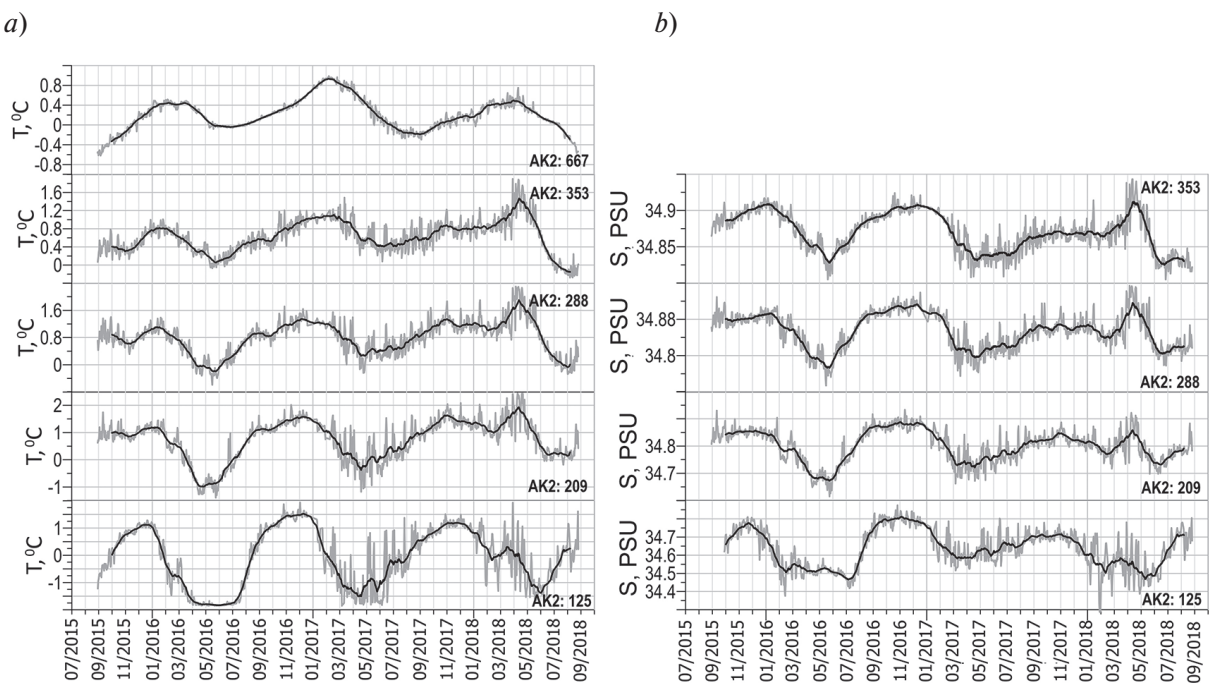

Fig. 5. Time series of temperature (*a*) and salinity (*b*) at all measured horizons in the upper 1000 m layer at AK2 AMS. Bold lines show the moving average with a 1-month smoothing window

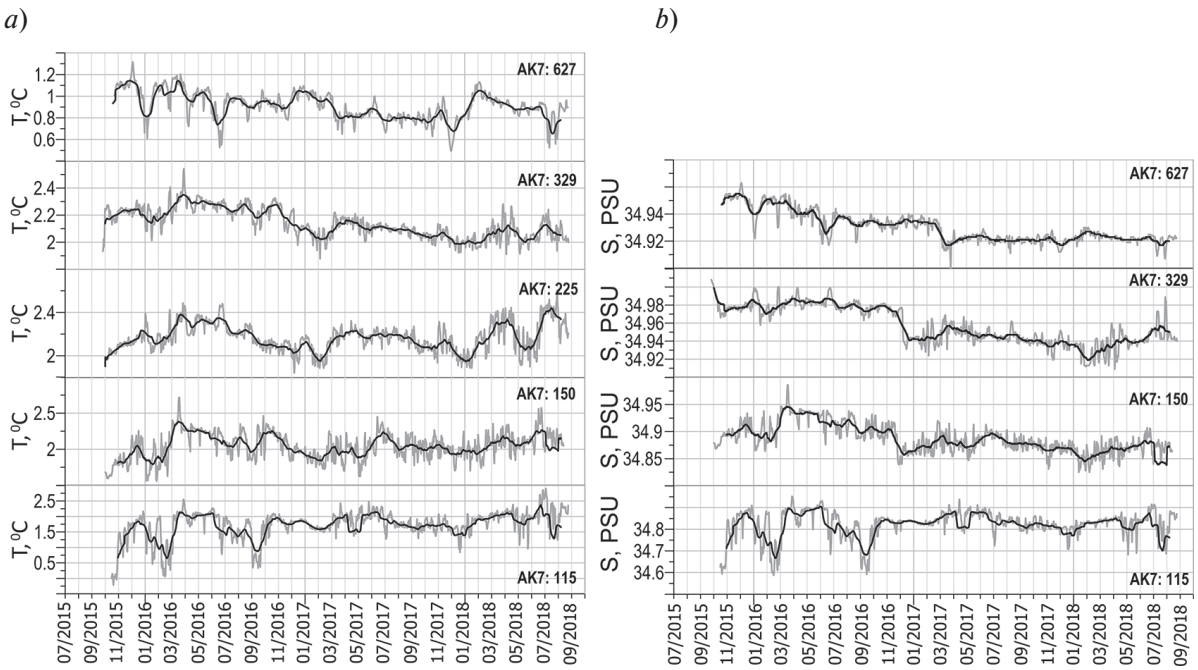

Fig. 6. Time series of temperature (*a*) and salinity (*b*) at all measured horizons in the upper 1000 m layer at AK7 AMS. Bold lines show the moving average with a 1-month smoothing window

In the "undisturbed" branch of FAW at AK7, vertical coherence in the temporal variability of thermohaline characteristics is considerably weaker. A visual resemblance in the time series marked by quasi-synchronous occurrence of annual minima and maxima is evident only for temperature at 225 and 329 m. In the salinity records, a consistent negative trend is apparent at both 329 and 627 m. For the remaining series at AK7, it is difficult to identify any distinct or coherent patterns.

Cross-correlation coefficients were also calculated for the time series at AMS AK2 and AK7, with the results presented in Tables 2 and 3. The significance level for all correlation coefficients (1 — p-value) exceeds 0.99.

At AMS AK2, high correlation coefficients (mostly above 0.5) are observed throughout the upper water layer from 125 to 353 m. In the core of the Atlantic Water (209–353 m), the correlation coefficients for values smoothed with a moving average reach 0.92–0.93. This indicates that the entire 125–353 m layer at AK2

Table 2

Cross-correlation coefficients for temperature series (above the diagonal) and salinity series (below the diagonal) on AK2 mooring

Depth, m	125	209	288	353	667
125	1	**0.79/0.83**	**0.56/0.62**	0.31/0.34	–0.01/–0.01
209	**0.69/070**	1	**0.88/0.92**	**0.64/0.67**	0.12/0.14
288	0.48/**0.51**	**0.87/0.94**	1	**0.86/0.89**	0.34/0.39
353	0.36/0.39	**0.72/0.79**	**0.88/0.93**	1	0.64/0.71
667	0.17/0.18	0.28/0.30	0.37/0.41	**0.55/0.60**	1

Note: "X/Y" indicates the correlation coefficient values for the daily and smoothed time series, respectively.

Table 3

Cross-correlation coefficients for temperature series (above the diagonal) and salinity series (below the diagonal) on AK7 mooring

Depth, m	115	150	225	329	627
115	1	0.30/0.48	0.35/0.29	0.01/0.12	0.06/–0/08
150	0.05/0.16	1	0.37/**0.51**	0.19/0.42	0.03/0.05
225	–	–	1	0.39/0.46	0.06/–0.09
329	0.06/–0.10	**0.67/0.84**	–	1	0.32/0.42
627	0.10/–0.11	**0.50/0.62**	–	**0.57/0.72**	1

Note: "X/Y" indicates the correlation coefficient values for the daily and smoothed time series, respectively.

represents a single water mass, with thermohaline properties varying under the influence of the same large-scale processes. Near the lower boundary of the Atlantic Water layer, this coherence weakens markedly, likely because the instrument at 667 m remained under the influence of Barents Atlantic Water throughout the observation period.

At AMS AK7, the situation is markedly different. Statistically significant correlation between temperature time series is observed only within the core of the Atlantic Water layer, and only for smoothed series with high-frequency variability filtered out. In the lower part of the Atlantic layer, a high correlation (above 0.5) is evident between salinity time series, but this is not the case for temperature series. As noted in the previous subsection, several instruments at different depths across various AMS were located within the Barents Atlantic Water influence zone.

This made it possible to assess the degree of coherence between the temperature time series recorded by these instruments (the salinity series were excluded from the analysis due to issues discussed in Section 2.1). The corresponding temperature series are shown in Fig. 7. Coherence among the records from AK1 (299 m), AK2 (667 m), and AK3 (599 m) which were under the influence of BAW both at deployment and at recovery is clearly evident visually. A pronounced annual cycle is present in these records, with temperature maxima occurring in February–March and minima in August–September. At AK4 (640 m) and AK5 (578 m), an initial period (up to approximately April 2016) is characterized by elevated temperatures (1.4 and 1.6 °C, respectively), after which a sharp drop is observed to 0.2 °C at AK4 and 0.6 °C at AK5 followed by persistently lower temperatures for the remainder of the record. Since the corresponding instruments were located within the FAW layer at the time of deployment but within the BAW layer at recovery (see Fig. 3), it is reasonable to assume that a sharp intensification of the BAW inflow occurred in April 2016, leading to the observed changes in the records. To test this hypothesis, cross-correlation coefficients were calculated between the time series shown in Fig. 7.

They are presented in Table 4. The significance level for all correlation coefficients (1 — p-value) exceeds 0.99. The high correlation coefficients for the temperature records at AK1, AK2, and AK3 indicate that the corresponding instruments at these AMS remained within the same water mass throughout the entire observation period, and that temporal temperature variations were driven by the same underlying processes.

The full temperature time series in the deep layer at AK4 and AK5 show virtually no correlation with the temperature series at AK1 and only weak correlation with those at AK2 and AK3. However, if the sharp and synchronous temperature drop recorded by these instruments in April 2016 (see Fig. 7) is taken into account and the correlation coefficients are recalculated with the initial segments of the series removed, the resulting coefficients increase significantly. For the smoothed records, two out of three exceed 0.5. This provides strong support for the earlier hypothesis that from May 2016 until recovery, the deep instruments at AK4 and AK5 remained within the BAW-influenced zone.

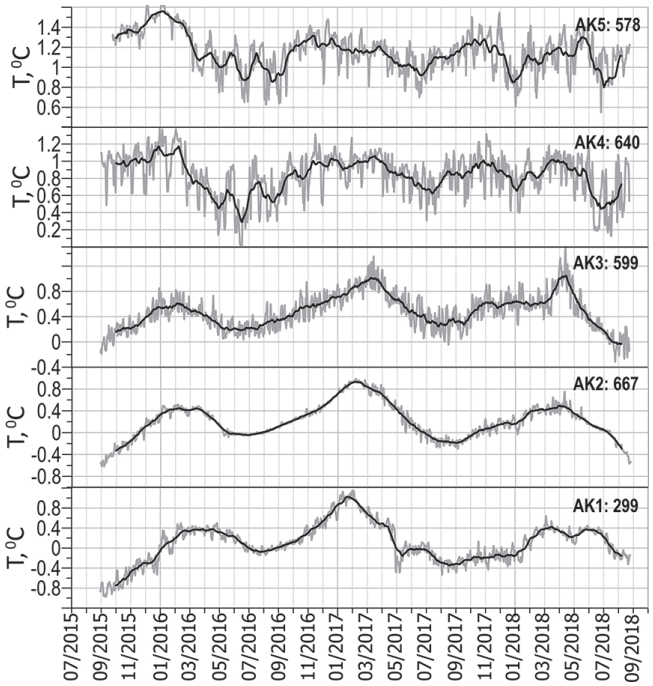

Fig. 7. Temperature time series at AK1–AK5 AMS, located in the zone influenced by BAW. Bold lines show the moving average with a 1-month smoothing window

Table 4

Cross-correlation coefficients for complete temperature series (above the diagonal) and temperature series with records before April 2016 removed (below the diagonal) on AMS located in the BAW influence zone

AMS - Depth, m	AK1–299	AK2–667	AK3–599	AK4–640	AK5–578
AK1–299	1	**0.84/0.87**	**0.53/0.64**	0.03/0.03	0.02/0.05
AK2–667	–	1	**0.77/0.88**	0.26/38	0.13/0.19
AK3–599	–	–	1	0.39/0.53	0.11/0.22
AK4–640	0.21/0.32	0.40/**0.59**	0.50/**0.78**	1	0.45/**0.74**
AK5–578	0.22/0.33	0.22/0.37	0.19/0.44	–	1

Note: "X/Y" indicates the correlation coefficient values for the daily and smoothed time series, respectively.

4.3. Spatiotemporal Variability of Thermohaline Properties from Model Simulations

Temperature and salinity time series were reproduced using the NEMO model at the locations of the seven AMS, at corresponding vertical levels and over the same time interval as the AMS cluster observations. Satisfactory agreement with the observational data was obtained only at the three shallowest AMS–AK1, AK2, and AK3located within the high-velocity core of the ABC [26]. At the other AMS, modelled temperature values were significantly underestimated relative to observations, and the temporal variability differed substantially from that observed. These discrepancies in the deep part of the basin are likely related to the weak current velocities [26, 41] at increasing distance from the ABC core. At current speeds of just 1–2 cm/s, even minor deviations between modelled and actual flow velocities can result in a reversal of water transport direction, which inevitably affects the thermohaline properties. Considering this, only AMS AK1–AK3 were used for

comparative analysis with the observations. Temporal variations in temperature and salinity at the temperature maximum layer (analogous to those shown in Fig. 4) from both the observations and NEMO model outputs are presented in Fig. 8. Salinity time series at AK1 are shown at 220 m, as the series at 299 m was deemed unreliable for the reasons discussed in Section 2.1.

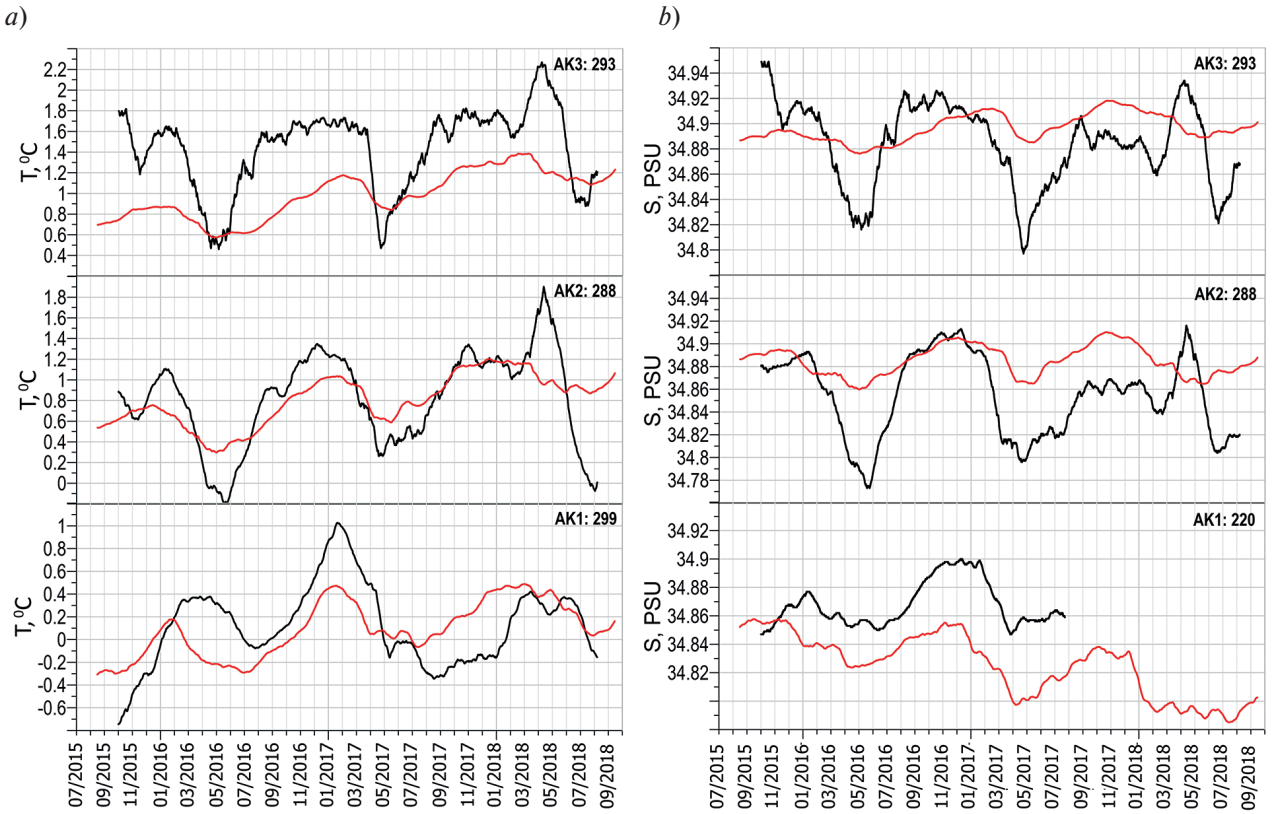

Fig. 8. Time series of 1-month moving average of temperature (*a*) and salinity (*b*) in the AW layer from observations (black lines) and the NEMO model (red lines). Mooring numbers and measurement depths are indicated in the figure

Overall, the model reproduces the large-scale variability in the thermohaline time series reasonably well, including the annual cycle. At AK2 and AK3, the phase of the intra-annual fluctuations in temperature and salinity matches the observations to within one month. At AK1, the timing of the temperature maximum in 2016 in the model leads the observed peak by about two months; however, this discrepancy decreases to about one month in subsequent years, consistent with the pattern seen at the other AMS. As expected, the amplitude of the annual fluctuations in the model output is lower than in the observations. This is clearly related to the fact that any numerical model inevitably smooths extremes to some degree due to the presence of model viscosity [42]. To quantitatively assess the parameters of the annual cycle and evaluate their agreement between the time series derived from in situ observations and model output, wavelet analysis was performed. For a more precise estimation of the annual cycle characteristics, wavelet analysis was applied to both the observational and model data. As an illustration, local wavelet power spectra of the temperature and salinity time series at 288 m depth are shown in Fig. 9.

All local wavelet power spectra of temperature and salinity, based on both observational and model data, show a prominent period close to one year (365 days). The dimensionless maxima of spectral density for both temperature and salinity in the observational data are approximately twice as large as those derived from the model and are statistically significant. The difference in the timing of the temperature and salinity maxima along

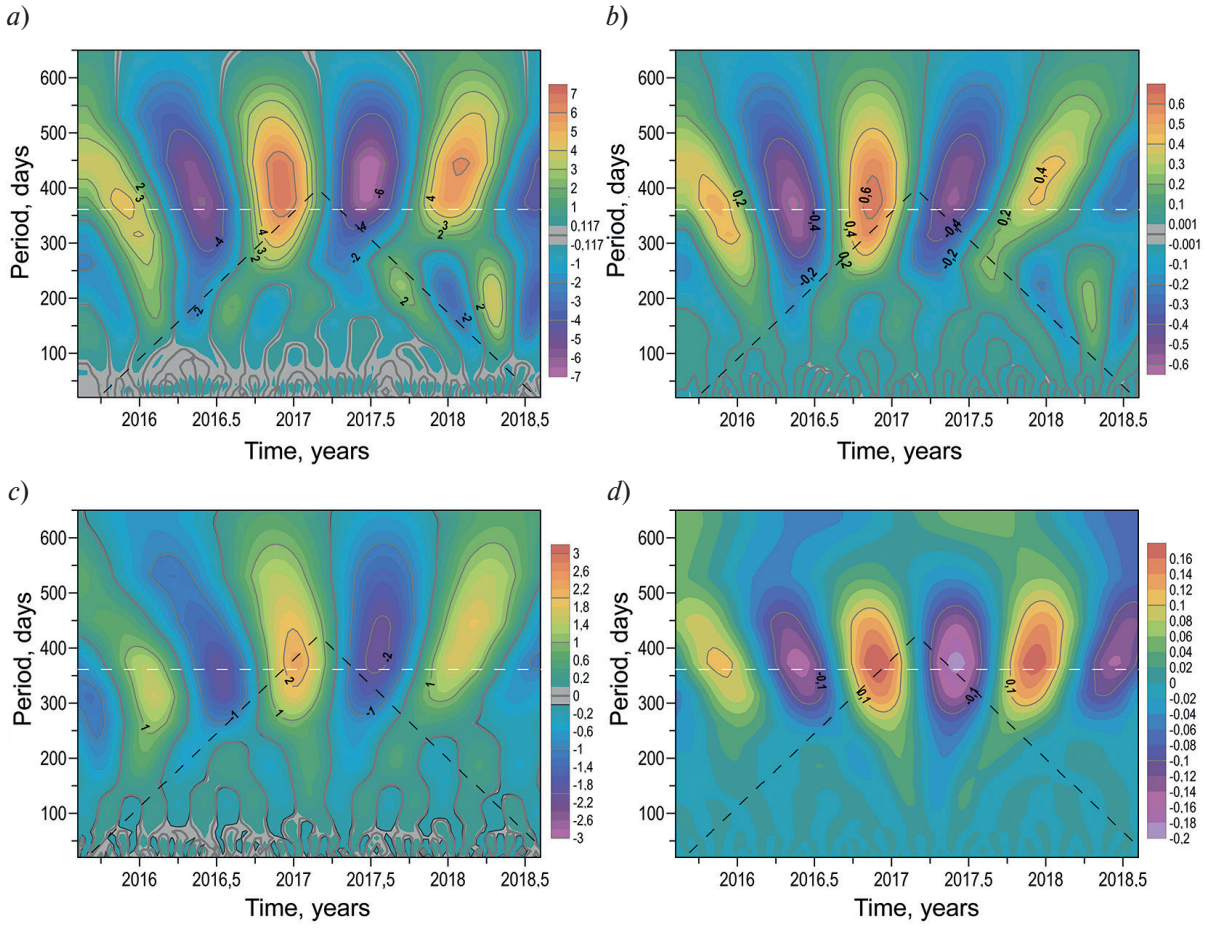

Fig. 9. The local wavelet power spectra of temperature (left) and salinity (right) at AK2 mooring at 288 m based on observations (*a*, *b*) and the NEMO model (*c*, *d*). The white dashed line marks the 365-day period. Shaded areas indicate regions with significance below 95 %. The cone of influence, where edge effects become important, is bounded above by the black dashed line

the time axis between the observational and model data does not exceed two months. According to the presented distributions, the annual cycle appears to be stationary, as it is clearly visible on the power spectra of both temperature and salinity, based on both observational and model data throughout the analyzed time interval. However, it should be noted that, formally, for much of the time series, the annual period falls within the region affected by edge effects, which is due to the limited duration of the observations. This implies that results lying above the so-called cone of influence (indicated by the black dashed line in Fig. 9) should be interpreted with caution. Nonetheless, the presence of such a cycle is fully consistent with the periodicity evident in the time series plots from the observations (see Figs. 4 and 5) and the NEMO model output (see Fig. 8), and therefore raises no doubt.

In summary, although the model output underestimates the amplitude of the observed seasonal variations, it accurately reproduces the oscillation period and shows satisfactory agreement with observations from the slope AMS AK1–AK3 in terms of phase. This indicates that the model data qualitatively capture the spatiotemporal variability of hydrographic fields within the high-velocity core of the ABC. This, in turn, provides a sound basis for using the numerical modeling results to test the hypothesis of advective transport of the seasonal signal across the entire eastern Atlantic sector of the AO.

5. Spatiotemporal Variability of AW Temperature in the Eastern Atlantic Sector of the AO

As demonstrated in the previous sections, coherent temperature oscillations with a period of approximately 12 months were observed at AK2, located in the core of the ABC, where the average current velocity exceeds 10 cm/s in the 125–288 m layer [26] (see Fig. 5a). Oscillations of the same period had previously been identified along the ABC pathway in other regions of the eastern Atlantic sector of the AO (see references in the Introduction). However, the phase of the temperature maximum defined here as the month when the water temperature in the upper FAW layer (from the 0 °C isotherm to the temperature maximum) reaches its peak varies across different regions. Between Svalbard and Franz Josef Land (30°E), the temperature maximum occurs in November [15]; on the western slope of the St. Anna Trough (around 60°E), it occurs in February [22]; and north of the Severnaya Zemlya (90°E), it falls in January (see Fig. 5).

The degree to which the observed sequence of phase changes aligns with the model results can be assessed using the maps of monthly mean water temperature at 135 m depth in the eastern Atlantic sector of the AO, shown in Fig. 10. These maps, based on the NEMO model output, cover the period from November 2016 to February 2018. The 135 m horizon was selected for illustration because the amplitude of the intra-annual temperature variability in the model is greatest at this depth.

We focus on three regions located along the FAW transport pathway: (1) between eastern Spitsbergen and the western slope of the Franz Victoria Trough (20–45°E); (2) the western slope of the St. Anna Trough and the adjacent continental slope to its northeast (60–70°E); and (3) the continental slope between the Voronin Trough and the northern tip of the Severnaya Zemlya Archipelago (80–95°E), which includes the AMS cluster. In addition, we consider region (4), where BAW enters the Nansen Basin, encompassing the eastern slope of the St. Anna Trough and the Voronin Trough in the Kara Sea. The locations of all four regions are shown in Fig. 1. In region 1, the maximum water temperature (4.9 °C)—the absolute maximum for the entire eastern AO sector — is observed in November 2016. In the following months, temperature gradually decreases, reaching a minimum (3 °C) in May 2017, after which it rises again to a new absolute maximum (4.8 °C) in November 2017. In region 2, the northward progression of the temperature front from November 2016 to January 2017 is clearly visible, with temperatures north of the St. Anna Trough reaching an annual maximum of 3 °C. Over the next two months, the area of warmer water within the St. Anna Trough expands, and an annual temperature maximum (2.5 °C) is reached at the boundary between the Barents and Kara seas. From May to July, temperatures in region 2 decrease to an annual minimum of 2.1 °C, followed by a renewed increase, reaching a maximum in January 2018. In region 3, a steady increase in temperature is observed from November 2016 (0.9 °C) to February 2017 (1.5 °C), followed by a decline to a minimum of 0.5 °C in May 2017. From June to November 2017, the temperature in region 3 increases again, reaching a new annual maximum of 1.6 °C in November 2017. This presents a clear discrepancy with the basic hypothesis, according to which the temperature rise in region 3 should occur in February–April, as the temperature front in the ABC flow shifts along the mouths of the St. Anna and Voronin troughs — something not observed in either the model results or the observational data (see Figs. 5 and 8). A possible explanation for this contradiction can be found by turning to region 4, where temperature changes reflect the characteristics of BAW transported into the Nansen Basin via the St. Anna Trough. The annual temperature maximum in region 4 is observed in November–December 2016. During these two months, relatively warm water (0.4–0.8 °C) completely fills the eastern slope of the St. Anna Trough and nearly the entire Voronin Trough. From February to June 2017, the temperature in region 4 decreases to its annual minimum (–0.8 °C), after which it begins to rise, reaching a maximum (0.8 °C) in November 2017. It is the result of intense mixing with cold BAW that explains the blocking of the eastward propagation of the FAW temperature front from February to July 2017—and even its reversal in April and May in region 3.

An additional argument in support of this explanation is provided by the temperature time series shown in Fig. 4. At AK3–AK5, a sharp and synchronous drop in temperature by 1–1.5 °C and in salinity by 0.08–0.12 PSU is observed in April 2017, whereas such an episode is absent at the AMS located farther from the shelf (AK6 and AK7). This contrast between the time series from the shallow and deep AMS likely marks the approximate boundary of the intrusion of cold and fresher BAW into the region occupied by FAW. Seaward of this boundary, the phase of the seasonal cycle remains unchanged, as if no BAW intrusion had occurred, with the annual temperature maximum in April–May (see Fig. 4). After the BAW temperature begins to rise in July 2017, the eastward

propagation of the warm FAW front resumes. The necessary conditions for intense mixing in region 3 are provided by the deceleration of the ABC transport in the area of isobath divergence (which is consistent with the model results), and the formation of quasi-stationary eddy structures at the mouth of the St. Anna Trough [43].

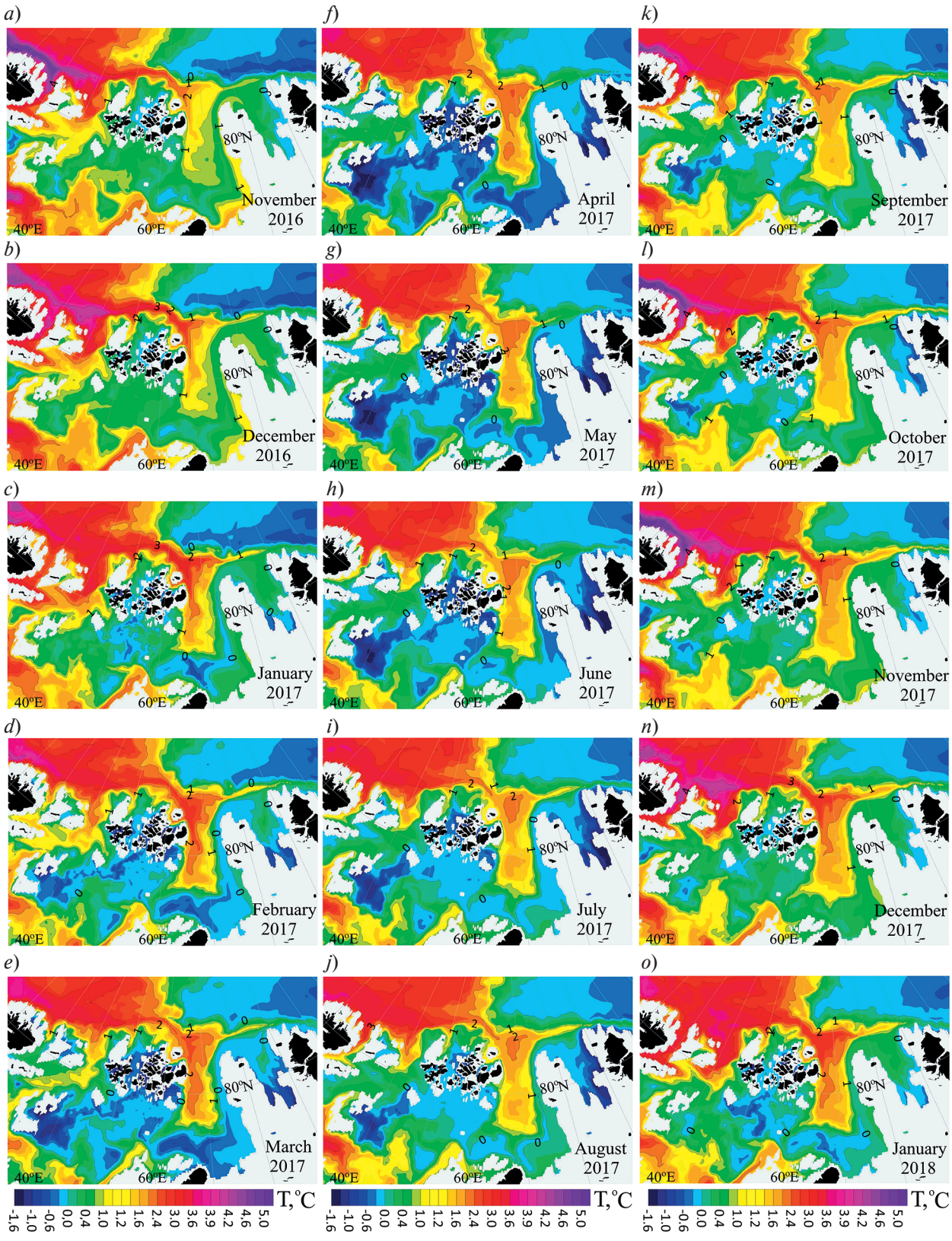

Fig. 10. Distribution of mean water temperature at the 135 m level based on NEMO model data from November 2016 to January 2018. Specific dates are indicated on the individual panels

Based on the phase shifts observed in regions 1–3, it is possible to roughly estimate the propagation speed of the temperature signal in the ABC between eastern Spitsbergen and the northern tip of the Severnaya Zemlya Archipelago. In section 1–2, it is close to the mean current speed, which at a depth of 135 m is about 10–15 cm/s according to model results. In section 2–3, the propagation speed of the temperature signal is approximately an order of magnitude lower. This is primarily due to the cooling of FAW from March to June as a result of mixing with BAW, and only secondarily due to the decrease in the zonal current component at the mouth of the St. Anna Trough, which, according to model estimates, drops to 3 cm/s at 135 m.

A strong flow of BAW along the eastern slope of the St. Anna Trough displaces the warm and saline core of FAW toward the northern periphery of the ABC (toward AK6 and AK7), occupying its place in the zone of maximum current velocity along the upper continental slope. Intense mixing across the front located in the area of AK2 and AK3 leads to a sharp cooling and freshening of the adjacent portion of the FAW core as far as AK5, and to a slight increase in temperature and salinity at AK1 in early April 2017 (see Fig. 4). By early July 2017, at the AMS AK4 and AK5, located farther from the front, temperature and salinity recover to values close to those observed at AK6 and AK7, while at the frontal AK2 and AK3 they retain intermediate characteristics between FAW and BAW.

6. Conclusion

The analysis of the spatiotemporal structure and variability of thermohaline parameters in the intermediate water layer of AW north of the Severnaya Zemlya Archipelago, based on data from AMS collected during 2015–2018, allows the following conclusions to be drawn:

Within 85 km of the shelf break, three distinct branches of AW are identified, each with its own history that governs the variability of its thermohaline properties. Directly at the shelf break (AK1) lies BAW, with a horizontal surface scale of 10–12 km, separated by a frontal zone less than 10 km wide (AK2–AK3) from the inner branch of FAW (AK4–AK5), which had recirculated in the northern part of the St. Anna Trough and exhibits a horizontal scale of about 40 km. In the abyssal region lies the outer ("undisturbed") branch of FAW (AK6–AK7), with a horizontal extent of at least 50 km.

The most energetic mode of temporal variability in thermohaline properties at all AMS is associated with intra-annual (seasonal) oscillations with a period of approximately 12 months. The amplitude of these oscillations decreases with distance from the shelf break, and the phase differs across the various AW branches. In individual branches, the phase may shift on an interannual timescale by up to ±1 month. No unidirectional trends were detected over the entire observation period; however, several events disrupted the regular pattern of variability, including a temperature increase across all AW branches in spring 2018 and a sharp drop in salinity in the outer branch of FAW during October–December 2016.

The model data obtained using the NEMO model for the 2015–2018 period allowed an assessment of how well the above conclusions align with the concept of a predominantly advective nature of the intra-annual temperature variability observed in FAW in the Nansen Basin [15, 20, 21, 22, 25]. Based on the results presented in Section 5, the following can be concluded:

– in the western part of the Nansen Basin (between Spitsbergen and the western slope of the St. Anna Trough), the phase shift of intra-annual temperature variations along the continental slope is controlled by the velocity of the ABC, as evidenced by the agreement between the propagation speed of the temperature signal and the modeled current velocity;

– the inflow of BAW through the St. Anna Trough disrupts this pattern. A strong BAW flow-comparable in volume transport to the AW inflow through the Fram Strait [44] displaces the FAW toward the northern periphery of the ABC, taking its place along the continental slope. Intense mixing across the front separating the BAW and the inner branch of the FAW leads to cooling/freshening of the latter. As a result, the timing of the temperature maximum in the inner branch of the FAW shifts forward by several months (ranging from 2 to 6 months depending on the distance from the front) compared to the timing of the maximum in the "undisturbed" outer branch of the FAW.

The conclusions presented above support several hypotheses about the propagation patterns of the seasonal temperature signal in the eastern part of the Nansen Basin, where this signal was also identified in instrumental observations [21, 24]. Since east of the St. Anna Trough, the BAW and the frontal part of the inner FAW branch are located in the region of high current velocity (in the upper part of the continental slope), the fastest prop-

agation of the seasonal temperature signal along with the preservation of a substantial oscillation amplitude is expected to occur within these branches. The outer FAW branch, where the absolute temperature maximum is found, is displaced to the northern periphery of the ABC, where current speeds are an order of magnitude lower than along the slope [26]. As a result, propagation of the temperature signal within the warm FAW core slows down (compared to the western Nansen Basin), the amplitude of seasonal variations decreases due to increased horizontal mixing, and the relative influence of other variability mechanisms becomes more significant. This is supported by observational data from the AMS in the Laptev Sea [24].

Funding

The study was carried out with support of the Russian Science Foundation grant No 24-17-00041.

References

1. Timofeev VT. *Water masses of the Arctic Basin*. L.: Gidrometeoizdat; 1960. 190 p. (in Russian).
2. GEBCO: The GEBCO_2023 Grid. Available from: https://www.gebco.net/data_and_products/gridded_bathymetry_data/gebco_2023/ (accessed 28 Apr 2024).
3. Nikiforov EG, Shpajxer AO. *Formation regularities of large-scale fluctuations of hydrological regime of the Arctic Ocean*. L.: Gidrometeoizdat; 1980. 270 p. (in Russian).
4. Aagaard K. A synthesis of Arctic Ocean circulation. *Rapports et Procès-Verbaux des Réunions du Conseil International pour l'Exploration de la Mer*. 1989;188:11–22.
5. Rudels B, Anderson LG, Jones E-P. Formation and evolution of the surface mixed layer and halocline of the Arctic Ocean. *Journal of Geophysical Research*: *Oceans*. 1996;101(C4):8807–8821. doi:10.1029/96JC00143
6. Rudels B, et al. Circulation and transformation of Atlantic water in the Eurasian Basin and the contribution of the Fram Strait inflow branch to the Arctic Ocean heat budget. *Progress in Oceanography*. 2015;132:128–152. doi:10.1016/j.pocean.2014.04.003
7. Schauer U, Loeng H, Rudels B, et al. Atlantic water flow through the Barents and Kara Seas. Deep-Sea Research Part I: Oceanographic Research Papers. 2002;49(12):2281–2298. doi:10.1016/S0967-0637(02)00125-5
8. Ivanov VV, Frolov IE, Filchuk KV. Transformation of Atlantic Water in the north-eastern Barents Sea in winter. *Arctic and Antarctic Research*. 2020;66(3):246–266.doi:10.30758/0555-2648-2020-66-3-246-266
9. Schauer U, Rudels B, Jones EP, et al. Confluence and redistribution of Atlantic Water in the Nansen, Amundsen and Makarov basins. *Annales Geophysicae*. 2002;20(2):257–273. doi:10.5194/angeo-20-257-2002
10. Ivanov VV, Aksenov EO. Atlantic water transformation in the eastern Nansen basin: observations and modeling. *Arctic and Antarctic Research*. 2013;1(95):72–87 (In Russian).
11. Quadfasel D, Sy A, Wells D, et al. A warming of the Arctic. *Nature*. 1991;359:385. doi:10.1038/350385a0
12. Alekseev GV, Bulatov LV, Zakharov VF, Ivanov VV. Intrusion of unusually warm Atlantic Water in the Arctic Ocean. *Reports of Russian Academy of Sciences*. 1997;356(3):401–403. (In Russian).
13. Polyakov I, Beszczynska A, Carmack EC, et al. One more step towards a warmer Arctic. *Geophysical Research Letters*. 2005;32: L17605. doi:10.1029/2005GL023740
14. Polyakov IV, et al. Observational program tracks Arctic Ocean transition to a warmer state. *Eos*, *Transactions*, *American Geophysical Union*. 2007;88(40):398–399. doi:10.1029/2007EO400002
15. Ivanov VV, Polyakov IV, Dmitrenko IA, et al. Seasonal variability in Atlantic Water off Spitsbergen. *Deep-Sea Research Part I*: *Oceanographic Research Papers*. 2009;56(1):1–14. doi:10.1016/j.dsr.2008.07.013
16. Ivanov V, Alexeev V, Koldunov NV, et al. Arctic Ocean heat impact on regional ice decay: a suggested positive feedback. *Journal of Physical Oceanography*. 2016;46(5):1437–1456. doi:10.1175/JPO-D-15-0144.1
17. Walczowski W, Piechura J. New evidence of warming propagating toward the Arctic Ocean. *Geophysical Research Letters*. 2006;33(12): L12601. doi:10.1029/2006GL025872
18. Holliday NP, Hughes SL, Bacon S, et al. Reversal of the 1960s to 1990s freshening trend in the northeast North Atlantic and Nordic Seas. *Geophysical Research Letters*. 2008;35(3): L03614. doi:10.1029/2007GL032675
19. Polyakov IV, Alexeev VA, Ashik IM, et al. NOWCAST: Fate of early-2000's Arctic warm water pulse. *Bulletin of the American Meteorological Society*. 2011;92(5):561–565. doi:10.1175/2010BAMS292I.1
20. Dmitrenko IA, Polyakov IV, Kirillov SA, et al. Seasonal variability of Atlantic water on the continental slope of the Laptev Sea during 2002–2004. *Earth and Planetary Science Letters*. 2006;244:735–743. doi:10.1016/j.epsl.2006.01.067
21. Dmitrenko I, Kirillov S, Ivanov V, et al. Seasonal modification of the Arctic Ocean intermediate water layer off the eastern Laptev Sea continental shelf break. *Journal of Geophysical Research*: *Oceans*. 2009;114: C06010. doi:10.1029/2008JC005229

22. Ivanov VV, Repina IA. The effect of seasonal variability of Atlantic water on the Arctic Sea ice cover. *Izvestiya, Atmospheric and Oceanic Physics*. 2018;54(1):65–72. doi:10.1134/S0001433818010061
23. Randelhof J, Ivanov V, et al. Seasonality of the physical and biogeochemical hydrography in the inflow to the Arctic Ocean through Fram Strait. Frontiers in Marine Science. 2018;5. doi:10.3389/fmars.2018.00224
24. Baumann TM, Polyakov IV, Pnyushkov AV, et al. On the seasonal cycles observed at the continental slope of the eastern Eurasian Basin of the Arctic Ocean. Journal of Physical Oceanography. 2018;48:1451–1470. doi:10.1175/JPO-D-17-0163.1
25. Renner AHH, Sundfjord A, Janout MA, et al. Variability and redistribution of heat in the Atlantic Water boundary current north of Svalbard. *Journal of Geophysical Research*: *Oceans*. 2018;123(9):6373–6391. doi:10.1029/2018JC013814
26. Ruiz-Castillo E, Janout M, Hölemann J, et al. Structure and seasonal variability of the Arctic Boundary Current north of Severnaya Zemlya. *Journal of Geophysical Research*: *Oceans*. 2023;128(1). doi:10.1029/2022JC018677
27. Lique C, Steele M. Where can we find a seasonal cycle of the Atlantic water temperature within the Arctic Basin? *Journal of Geophysical Research*: *Oceans*. 2012;117: C03026. doi:10.1029/2011JC007612
28. Ivanov V, Maslov P, Aksenov Ye, et al. Shelf-basin exchange in the Laptev Sea in the warming climate: a model study. *Geophysical & Astrophysical Fluid Dynamics*. 2015;109:254–280. doi:10.1080/03091929.2015.1025776
29. Dmitrenko IA, Rudels B, Kirillov SA, et al. Atlantic water flow into the Arctic Ocean through the St. Anna Trough in the northern Kara Sea. *Journal of Geophysical Research*: *Oceans*. 2015;120(7):5158–5178. doi:10.1002/2015JC010804
30. Woodgate RA, Aagaard K, Muench RD, et al. The Arctic Ocean boundary current along the Eurasian slope and the adjacent Lomonosov Ridge: Water mass properties, transports and transformations from moored instruments. *Deep-Sea Research Part I*: *Oceanographic Research Papers*. 2001;48:1757–1792. doi:10.1016/S0967-0637(00)00091-1
31. NEMO Community Ocean Model. Available from: https://www.nemo-ocean.eu/. (Accessed April 17, 2023).
32. Sea-Bird Scientific. Available from: https://www.seabird.com/ (Accessed August 28, 2024).
33. Zenodo: NEMO shared references. NEMO ocean engine. Version v3.6-patch. Available from: https://zenodo.org/records/3248739 (Accessed March 25, 2023). doi:10.5281/zenodo.3248739
34. LIM. The Louvain-la-Neuve sea Ice Model. Available from: https://cmc.ipsl.fr/images/publications/scientific_notes/lim3_book.pdf (Accessed March 25, 2023).
35. Copernicus Marine Service: Ocean products. Global Ocean Physics Reanalysis. Available from: https://data.marine.copernicus.eu/product/GLOBAL_MULTIYEAR_PHY_001_030/services (Accessed December 1, 2022).
36. ECMWF: ECMWF Reanalysis v5 (ERA5). Available from: https://www.ecmwf.int/en/forecasts/dataset/ecmwf-reanalysis-v5 (Accessed September 17, 2023).
37. Egbert DG, Erofeeva SY. Efficient inverse modelling of barotropic ocean tides. Journal of Atmospheric and Oceanic Technology. 2002;19(2):182–204. doi:10.1175/1520-0426(2002)019
38. World Ocean Database and World Ocean Atlas Series. WOA18.DATA. Available from: https://www.ncei.noaa.gov/data/oceans/woa/WOA18/DATA/ (Accessed February 8, 2021).
39. Emery WJ, Thomson RE. Data Analysis Methods in Physical Oceanography. New York: Elsevier; 2004. 637 p.
40. University of Bremen. Sea Ice Concentration. AMSR-E/AMSR2. Available from: https://seaice.uni-bremen.de/sea-ice-concentration/amsre-amsr2 (Accessed February 8, 2023).
41. Pnyushkov AV, Polyakov IV, Alekseev GV, et al. A steady regime of volume and heat transports in the eastern Arctic Ocean in the early 21st century. Frontiers in Marine Science. 2021;8:705608. doi:10.3389/fmars.2021.705608
42. Marchuk GI, Dymnikov VP, Zalesnyj VB. Mathematical models in geophysical hydrodynamics and numerical methods for their implementation. L.: Gidrometeoizdat; 1987. 295 p. (In Russian).
43. Osadchiev A, Viting K, Frey D, et al. Structure and circulation of Atlantic water masses in the St. Anna Trough in the Kara Sea. *Frontiers in Marine Science*. 2022;9:915674. doi:10.3389/fmars.2022.915674
44. Rudels B. Arctic Ocean circulation and variability — advection and external forcing encounter constraints and local processes. Ocean Science. 2012;8:261–286. doi:10.5194/os-8-261-2012

Литература

1. *Тимофеев В.Т.* Водные массы Арктического бассейна. Л.: Гидрометеоиздат, 1960. 190 с.
2. GEBCO: The GEBCO_2023 Grid. URL: https://www.gebco.net/data_and_products/gridded_bathymetry_data/gebco_2023/ (дата обращения: 28.04.2024).
3. *Никифоров Е.Г.*, *Шпайхер А.О.* Закономерности формирования крупномасштабных колебаний гидрологического режима Северного Ледовитого океана. Л.: Гидрометеоиздат, 1980. 270 с.
4. *Aagaard K.* A synthesis of Arctic Ocean circulation // Rapports et Procès-Verbaux des Réunions du Conseil International pour l'Exploration de la Mer. 1989. No. 188. P. 11–22.

5. *Rudels B.*, *Anderson L.G.*, *Jones E.-P.* Formation and evolution of the surface mixed layer and halocline of the Arctic Ocean // Journal of Geophysical Research: Oceans. 1996. Vol. 101, C4. P. 8807–8821. doi:10.1029/96JC00143
6. *Rudels B.*, et al. Circulation and transformation of Atlantic water in the Eurasian Basin and the contribution of the Fram Strait inflow branch to the Arctic Ocean heat budget // Progress in Oceanography. 2015. Vol. 132. P. 128–152. doi:10.1016/j.pocean.2014.04.003 EDN: UFPUAT
7. *Schauer U.*, *Loeng H.*, *Rudels B.*, et al. Atlantic water flow through the Barents and Kara Seas // Deep-Sea Research Part I: Oceanographic Research Papers. 2002. Vol. 49, No. 12. P. 2281–2298. doi:10.1016/S0967-0637(02)00125-5 EDN: LHNSFF
8. *Ivanov V.V.*, *Frolov I.E.*, *Filchuk K.V.* Transformation of Atlantic Water in the north-eastern Barents Sea in winter // Проблемы Арктики и Антарктики. 2020. Т. 66, № 3. С. 246–266. doi:10.30758/0555-2648-2020-66-3-246-266 EDN: EJDFSE
9. *Schauer U.*, *Rudels B.*, *Jones E.P.*, et al. Confluence and redistribution of Atlantic Water in the Nansen, Amundsen and Makarov basins // Annales Geophysicae. 2002. Vol. 20, No. 2. P. 257–273. doi:10.5194/angeo-20-257-2002 EDN: LHGZBJ
10. *Иванов В.В.*, *Аксенов Е.О.* Трансформация Атлантической воды в восточной части котловины Нансена по данным наблюдений и моделирования // Проблемы Арктики и Антарктики. 2013. № 1(95). С. 72–87. EDN: QIKULT
11. *Quadfasel D.*, *Sy A.*, *Wells D.*, et al. A warming of the Arctic // Nature. 1991. Vol. 359. P. 385. doi:10.1038/350385a0
12. *Алексеев Г.В.*, *Буматов Л.В.*, *Захаров В.Ф.* и др. Поступление необычно теплых атлантических вод в Арктический бассейн // Доклады Академии Наук. 1997. Т. 356, № 3. С. 401–403.
13. *Polyakov I.*, *Beszczynska A.*, *Carmack E.C.*, et al. One more step towards a warmer Arctic // Geophysical Research Letters. 2005. Vol. 32. L17605. doi:10.1029/2005GL023740
14. *Polyakov I.V.*, et al. Observational program tracks Arctic Ocean transition to a warmer state // Eos, Transactions, American Geophysical Union. 2007. Vol. 88, No. 40. P. 398–399. doi:10.1029/2007EO400002 EDN: LKUVKH
15. *Ivanov V.V.*, *Polyakov I.V.*, *Dmitrenko I.A.*, et al. Seasonal variability in Atlantic Water off Spitsbergen // Deep-Sea Research Part I: Oceanographic Research Papers. 2009. Vol. 56, No. 1. P. 1–14. doi:10.1016/j.dsr.2008.07.013 EDN: LLQADX
16. *Ivanov V.*, *Alexeev V.*, *Koldunov N.V.* et al. Arctic Ocean Heat Impact on Regional Ice Decay: A Suggested Positive Feedback // Journal of Physical Oceanography. 2016. Vol. 46, No. 5. P. 1437–1456. doi:10.1175/JPO-D-15-0144.1 EDN: WWEWCH
17. *Walczowski W.*, *Piechura J.* New evidence of warming propagating toward the Arctic Ocean // Geophysical Research Letters. 2006. Vol. 33, No. 12. L12601. doi:10.1029/2006GL025872 EDN: MJVDJZ
18. *Holliday N.P.*, *Hughes S.L.*, *Bacon S.*, et al. Reversal of the 1960s to 1990s freshening trend in the northeast North Atlantic and Nordic Seas // Geophysical Research Letters. 2008. Vol. 35, No 3. L03614. doi:10.1029/2007GL032675 EDN: MJVDRR
19. *Polyakov I.V.*, *Alexeev V.A.*, *Ashik I.M.*, et al. NOWCAST: Fate of early-2000's Arctic warm water pulse // Bulletin of the American Meteorological Society. 2011. Vol. 92, No. 5. P. 561–565. doi:10.1175/2010BAMS292I.1 EDN: OICOZB
20. *Dmitrenko I.A.*, *Polyakov I.V.*, *Kirillov S.A.*, et al. Seasonal variability of Atlantic water on the continental slope of the Laptev Sea during 2002–2004 // Earth and Planetary Science Letters. 2006. Vol. 244. P. 735–743. doi:10.1016/j.epsl.2006.01.067 EDN: LJXBMD
21. *Dmitrenko I.*, *Kirillov S.*, *Ivanov V.*, et al. Seasonal modification of the Arctic Ocean intermediate water layer off the eastern Laptev Sea continental shelf break // Journal of Geophysical Research: Oceans. 2009. Vol. 114, C06010. doi:10.1029/2008JC005229 EDN: TRNUTK
22. *Иванов В.В.*, *Репина И.А.* Влияние сезонной изменчивости атлантической воды на ледяной покров Северного Ледовитого океана // Известия Российской академии наук. Физика атмосферы и океана. 2018. Т. 54. № 1. С. 73–82. doi:10.7868/S0003351518010087 EDN: YOFWPH
23. *Randelhof J.*, *Ivanov V.*, et al. Seasonality of the Physical and Biogeochemical Hydrography in the Inflow to the Arctic Ocean Through Fram Strait // Frontiers in Marine Science. 2018. Vol. 5. doi:10.3389/fmars.2018.00224 EDN: VBPBEC
24. *Baumann T.M.*, *Polyakov I.V.*, *Pnyushkov A.V.*, et al. On the seasonal cycles observed at the continental slope of the Eastern Eurasian Basin of the Arctic Ocean // Journal of Physical Oceanography. 2018. Vol. 48. P. 1451–1470. doi:10.1175/JPO-D-17–0163.1 EDN: SBJDWL
25. *Renner A.H.H.*, *Sundfjord A.*, *Janout M.A.*, et al. Variability and redistribution of heat in the Atlantic Water boundary current north of Svalbard // Journal of Geophysical Research: Oceans. 2018. Vol. 123, No. 9. P. 6373–6391. doi:10.1029/2018JC013814 EDN: RULRFC
26. *Ruiz-Castillo E.*, *Janout M.*, *Hölemann J.*, et al. Structure and seasonal variability of the Arctic Boundary Current north of Severnaya Zemlya // Journal of Geophysical Research: Oceans. 2023. Vol. 128, No. 1. doi:10.1029/2022JC018677 EDN: ULSVPB
27. *Lique C.*, *Steele M.* Where can we find a seasonal cycle of the Atlantic water temperature within the Arctic Basin? // Journal of Geophysical Research: Oceans. 2012. Vol. 117. C03026. doi:10.1029/2011JC007612 EDN: DQICUU

28. *Ivanov V.*, *Maslov P.*, *Aksenov Ye.*, et al. Shelf-Basin Exchange in the Laptev Sea in the Warming Climate: a model study // Geophysical & Astrophysical Fluid Dynamics. 2015. Vol. 109. P. 254–280. doi:10.1080/03091929.2015.1025776 EDN: UESKGL
29. *Dmitrenko I.A.*, *Rudels B.*, *Kirillov S.A.*, et al. Atlantic water flow into the Arctic Ocean through the St. Anna Trough in the northern Kara Sea // Journal of Geophysical Research: Oceans. 2015. Vol. 120, No. 7. P. 5158–5178. doi:10.1002/2015JC010804 EDN: UOJCXL
30. *Woodgate R.A.*, *Aagaard K.*, *Muench R.D.*, et al. The Arctic Ocean boundary current along the Eurasian slope and the adjacent Lomonosov Ridge: Water mass properties, transports and transformations from moored instruments // Deep-Sea Research Part I: Oceanographic Research Papers. 2001. Vol. 48. P. 1757–1792. doi:10.1016/S0967-0637(00)00091-1 EDN: LYTTRT
31. NEMO Community Ocean Model. URL: https://www.nemo-ocean.eu/ (дата обращения: 17.04.2023).
32. Sea-Bird Scientific. URL: https://www.seabird.com/ (дата обращения: 28.08.2024).
33. Zenodo: NEMO shared references. NEMO ocean engine. Version v3.6-patch. URL: https://zenodo.org/records/3248739 (дата обращения: 25.03.2023). doi:10.5281/zenodo.3248739
34. LIM. The Louvain-la-Neuve sea Ice Model. URL: https://cmc.ipsl.fr/images/publications/scientific_notes/lim3_book.pdf (дата обращения: 25.03.2023).
35. Copernicus Marine Service: Ocean products. Global Ocean Physics Reanalysis. URL: https://data.marine.copernicus.eu/product/GLOBAL_MULTIYEAR_PHY_001_030/services (дата обращения: 01.12.2022).
36. ECMWF: ECMWF Reanalysis v5 (ERA5). URL: https://www.ecmwf.int/en/forecasts/dataset/ecmwf-reanalysis-v5 (дата обращения: 17.09.2023).
37. *Egbert D.G.*, *Erofeeva S.Y.* Efficient inverse modelling of barotropic ocean tides // Journal of Atmospheric and Oceanic Technology. 2002. Vol. 19, No. 2. P. 182–204. <0183: EIMOBO>2.0.CO;2. doi:10.1175/1520-0426(2002)019
38. World Ocean Database and World Ocean Atlas Series. WOA18.DATA. URL: https://www.ncei.noaa.gov/data/oceans/woa/WOA18/DATA/ (дата обращения: 08.02.2021).
39. *Emery W.J.*, *Thomson R.E.* Data Analysis Methods in Physical Oceanography. New York: Elsevier, 2004. 637 p.
40. University of Bremen. Sea Ice Concentration. AMSR-E/AMSR2. URL: https://seaice.uni-bremen.de/sea-ice-concentration/amsre-amsr2 (дата обращения: 08.02.2023).
41. *Pnyushkov A.V.*, *Polyakov I.V.*, *Alekseev G.V.* et al. A Steady Regime of Volume and Heat Transports in the Eastern Arctic Ocean in the Early 21st Century // Frontiers in Marine Science. 2021. Vol. 8. 705608. doi:10.3389/fmars.2021.705608 EDN: QXKYIL
42. *Марчук Г.И.*, *Дымников В.П.*, *Залесный В.Б.* Математические модели в геофизической гидродинамике и численные методы их реализации. Л.: Гидрометеоиздат, 1987. 295 с.
43. *Osadchiev A.*, *Viting K.*, *Frey D.*, et al. Structure and circulation of Atlantic water masses in the St. Anna Trough in the Kara Sea // Frontiers in Marine Science. 2022. Vol. 9. 915674. doi:10.3389/fmars.2022.915674 EDN: FPFVEH
44. *Rudels B.* Arctic Ocean circulation and variability — advection and external forcing encounter constraints and local processes // Ocean Science. 2012. Vol. 8. P. 261–286. doi:10.5194/os-8-261-2012 EDN: RJXZJV

About the Authors

VLADIMIR V. Ivanov, Chief Researcher, M.V. Lomonosov Moscow State University, Arctic and Antarctic Research Institute, DrSc. (Phys.-Math.), ORCID: 0000-0003-2569-6027, Scopus AuthorID: 57203338116, WoS ResearcherID: J-5979–2014, SPIN-код (РИНЦ): 9424-7920, e-mail: vladimir.ivanov@aari.ru

ANNA V. Danshina, Senior Researcher, Arctic and Antarctic Research Institute, CandSc. (Phys.-Math.), ORCID: 0000-0002-5741-9801, Scopus AuthorID: 55781395200, WoS ResearcherID: AEG-1081–2022, SPIN-код (РИНЦ): 2725-4600, e-mail: danshina@aari.ru

ALEXANDER V. Smirnov, Senior Researcher Arctic and Antarctic Research Institute, CandSc. (Geogr.), ORCID: 0000-0003-3231-7283, Scopus AuthorID: 56264603400, WoS ResearcherID: J-5935–2014, SPIN-код (РИНЦ): 4473-2959, e-mail: alexander.vic.smirnov@gmail.com